



**University of
Zurich**^{UZH}

**Zurich Open Repository and
Archive**

University of Zurich
University Library
Strickhofstrasse 39
CH-8057 Zurich
www.zora.uzh.ch

Year: 2020

Quantitative intravital calcium imaging maps single cell behavior to kidney tubular structure

Martins, Joana Raquel ; Haenni, Dominik ; Bugarski, Milica ; Figurek, Andreja ; Hall, Andrew M

DOI: <https://doi.org/10.1152/ajprenal.00052.2020>

Posted at the Zurich Open Repository and Archive, University of Zurich

ZORA URL: <https://doi.org/10.5167/uzh-188175>

Journal Article

Supplemental Material

Originally published at:

Martins, Joana Raquel; Haenni, Dominik; Bugarski, Milica; Figurek, Andreja; Hall, Andrew M (2020). Quantitative intravital calcium imaging maps single cell behavior to kidney tubular structure. *American Journal of Physiology: Renal Physiology*, 319(2):F245-F255.

DOI: <https://doi.org/10.1152/ajprenal.00052.2020>

Supplementary Materials

Quantitative intravital calcium imaging maps single cell behavior to kidney tubular structure

Martins JR¹, Haenni D^{1,2}, Bugarski M¹, Figurek A¹, Hall AM^{1,3}.

¹Institute of Anatomy, University of Zurich, Switzerland. ²Center for Microscopy and Image Analysis, University of Zurich, Switzerland. ³Department of Nephrology, University Hospital Zurich, Switzerland.

Correspondence to: andrew.hall@uzh.ch

This file includes:

Figures S1 to S6 and corresponding figure legends

Captions for Movies S1 to S5 (available at <https://figshare.com/s/537b33e39b507142e525>)

Supplementary Material and Methods

Table of contents

Fig. S1. GCaMP6s is expressed throughout the kidney tubule.

Fig. S2. Calcium transients originate apically and propagate towards the basolateral side of proximal tubule cells.

Fig. S3. Photo-induced calcium rises occur at higher laser powers in specific tubular segments.

Fig. S4. Monitoring GCaMP6s signal using automated cell localization is representative of changes in kidney proximal tubule cells.

Fig. S5. GCaMP6s is not saturated under physiological conditions.

Fig. S6. Effect of candesartan on calcium transients in the proximal tubule.

Movie S1. Co-imaging of calcium signaling and mitochondrial function in kidney proximal tubule cells.

Movie S2. Calcium transients originate apically and propagate towards the basolateral side of proximal tubule cells.

Movie S3. Calcium transients in proximal tubules display a cyclical pattern in activation probability.

Movie S4. Proximal tubular cells show altered calcium signaling in cisplatin induced

AKI.

Movie S5. Cellular material is shed into tubular lumens in cisplatin induced AKI.

Supplementary Material and Methods

Fig. S1

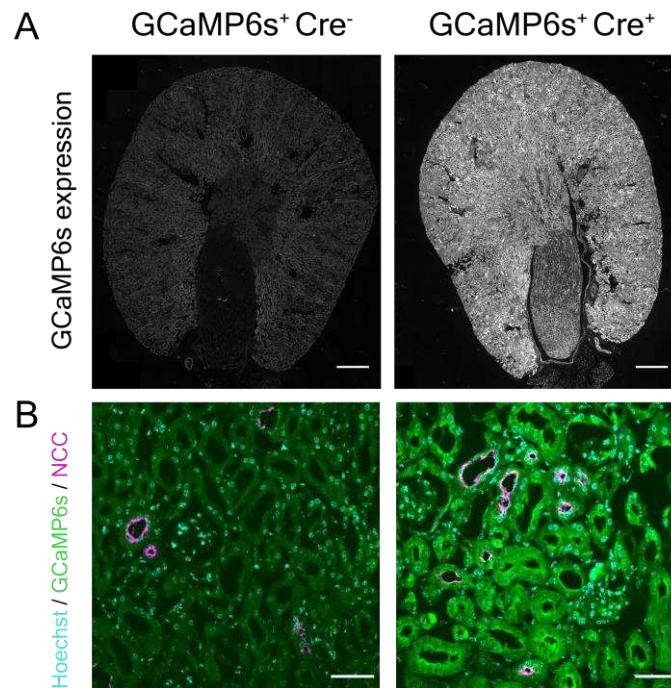


Fig. S1. GCaMP6s is expressed throughout the kidney tubule. (A) Immunostained $GCaMP6s^{+}Cre^{+}$ kidney sections reveals that the Ca^{2+} sensitive probe GCaMP6s is expressed throughout the kidney (gray), but not in kidney sections from $GCaMP6s^{+}Cre^{-}$ mice. Scale bar, 500 μm . (B) Representative confocal images of immunofluorescence stainings of GCaMP6s (green) and the NaCl cotransporter (NCC, magenta) from $GCaMP6s^{+}Cre^{-}$ and $GCaMP6s^{+}Cre^{+}$ mice showing the probe is expressed in the distal convoluted tubule. Scale bar, 50 μm .

Fig. S2

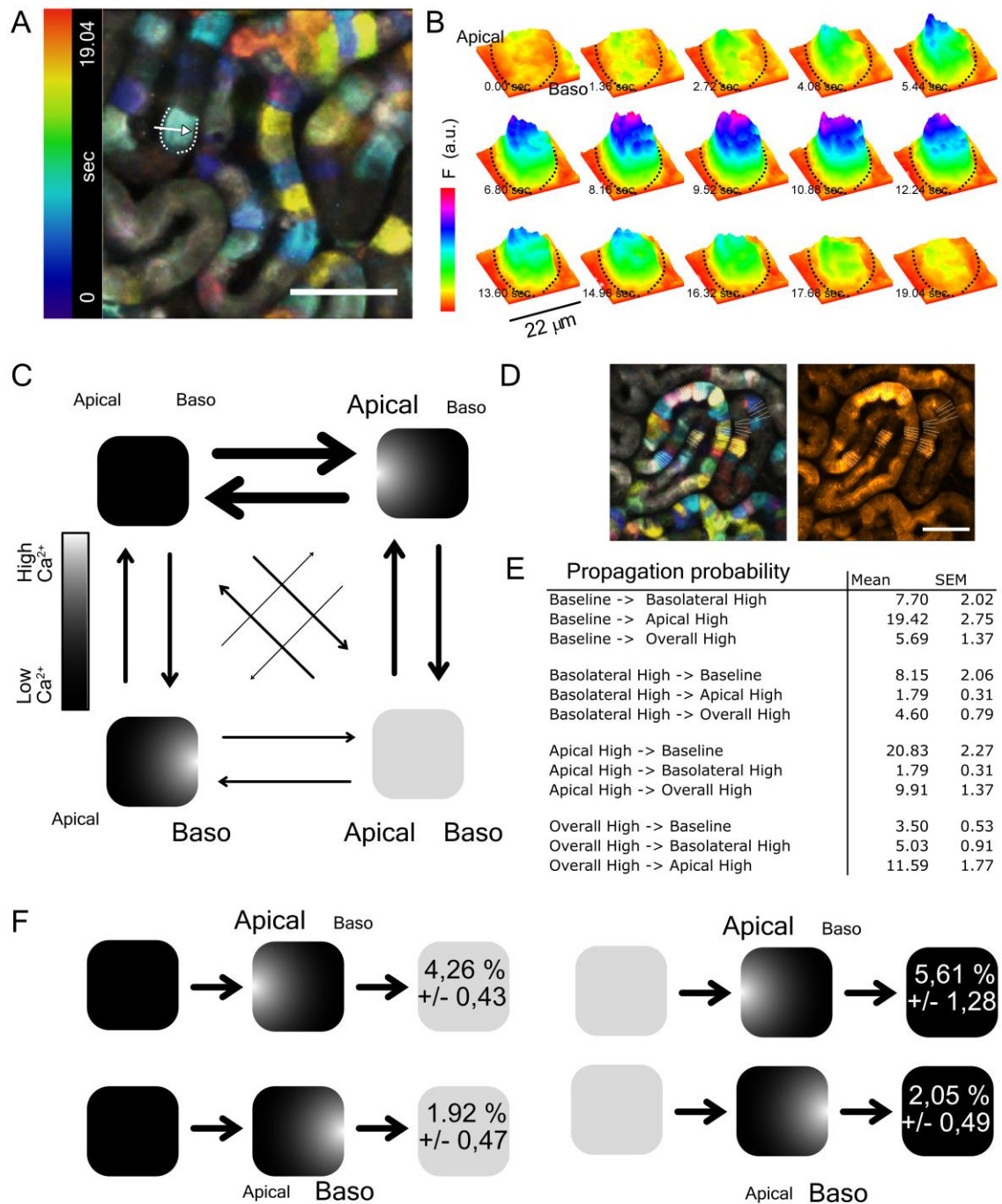


Fig. S2. Calcium transients originate apically and propagate towards the basolateral side of proximal tubule cells. (A) GCaMP6s temporal color coded image (Scale bar, 50 μ m) and **(B)** surface intensity plot of a labelled cell showing that Ca^{2+} transients *in vivo* originate at the apical side (Apical) and propagate towards the basolateral side (Baso) of a proximal tubule cell

(direction indicated by arrow). **(C)** Illustration of the different Ca^{2+} distribution transition states. Size of the arrows reflects the contribution of each transition. **(D)** Line ROIs spanning the cell from the apical to the basolateral side were manually drawn illustrating how the analysis was performed. GCaMP6s temporal color coded image (30sec) – left, and integrated GCaMP6s signal – right. **(E)** Probability of the different transitions in S1 cells. **(F)** Probability of the different triple transitions (\pm SEM) in S1 cells. Ca^{2+} transients are more likely to propagate through the apical side of the cell. Results were summarized from 30 different S1 cells, from 6 independent recordings. Images were acquired at the rate of 1 frame per 0.68 sec.

Fig. S3

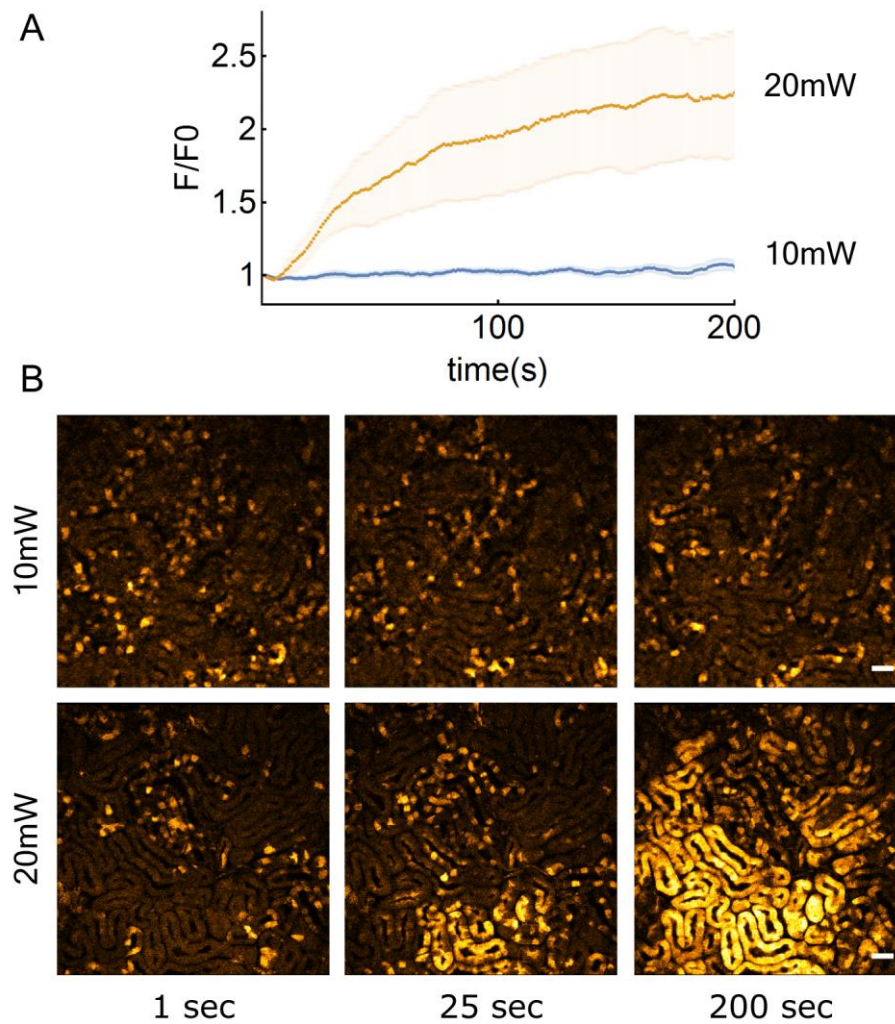


Fig. S3. Photo-induced calcium rises occur at higher laser powers in specific tubular segments. (A) Normalized GCaMP6s fluorescence dramatically increases in a subset of tubules when intravital imaging is performed at 20 mW (measured at the sample). Experiments were subsequently performed at a maximum of 10 mW in order to achieve minimal photo-induced effects while still retaining enough signal for further analysis (Mean \pm SEM, from a minimum of 3 independent intravital imaging experiments). (B) Representative images of intravital imaging of GCaMP6s kidneys performed at 10 or 20 mW. The tubules with higher sensitivity were subsequently identified as S2 proximal tubules based on their auto fluorescence profiles. Scale bar, 50 μ m.

Fig. S4

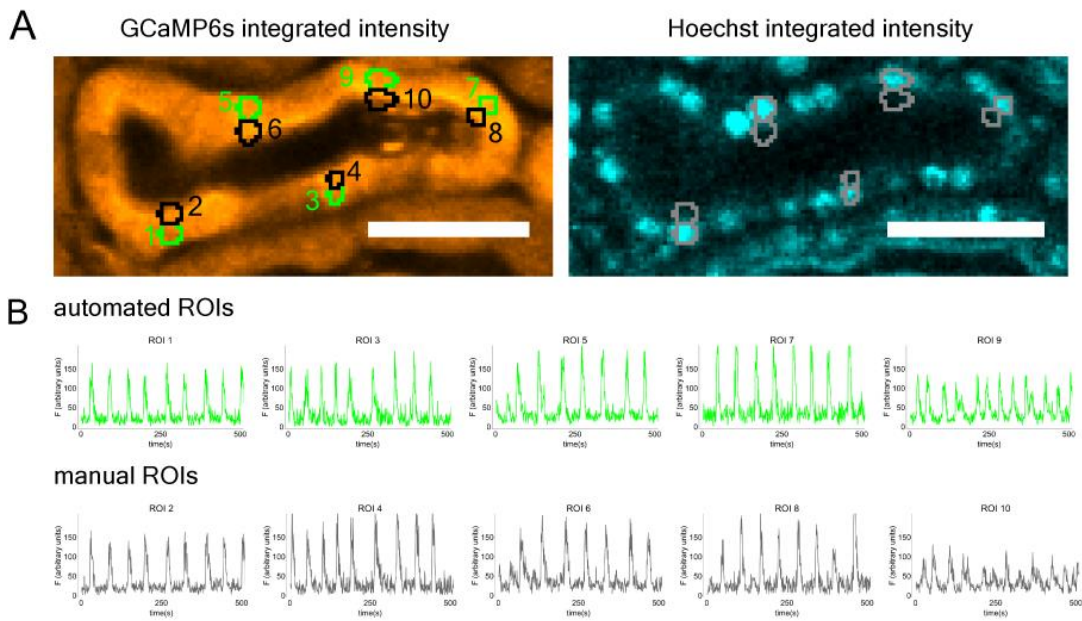


Fig. S4. Monitoring GCaMP6s signal using automated cell localization is representative of changes in kidney proximal tubule cells. (A) To validate whether automatically detected regions of interest (ROIs) using the integrated Hoechst signal (ROIs in green) were representative of GCaMP6s signal throughout the cell, traces were compared to manually placed ROIs in other locations (in black). **(B)** GCaMP6s traces corresponding to automatically detected ROIs (green) or manually placed ROIs (black). Frequency and duration of transients was comparable using the two approaches. Scale bar, 50 μm .

Fig. S5

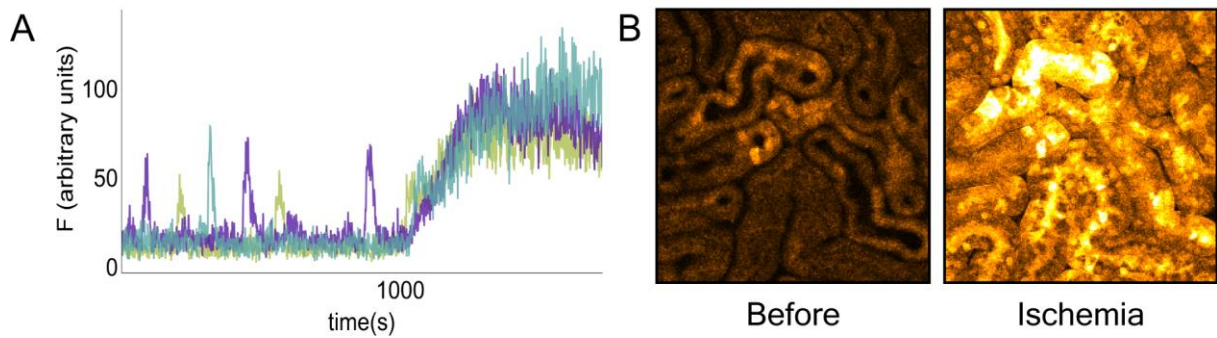


Fig. S5. GCaMP6s is not saturated under physiological conditions. (A) Fluorescence intensity in GCaMP6s kidney proximal tubules increases upon cessation of circulation (ischemia) to higher levels than observed during physiological transients. Each single trace represents changes in GCaMP6s fluorescence in individual cells from different tubules. (B) Representative images of GCaMP6s intensity in proximal tubules before and after ischemia. Scale bar, 50 μm .

Fig. S6

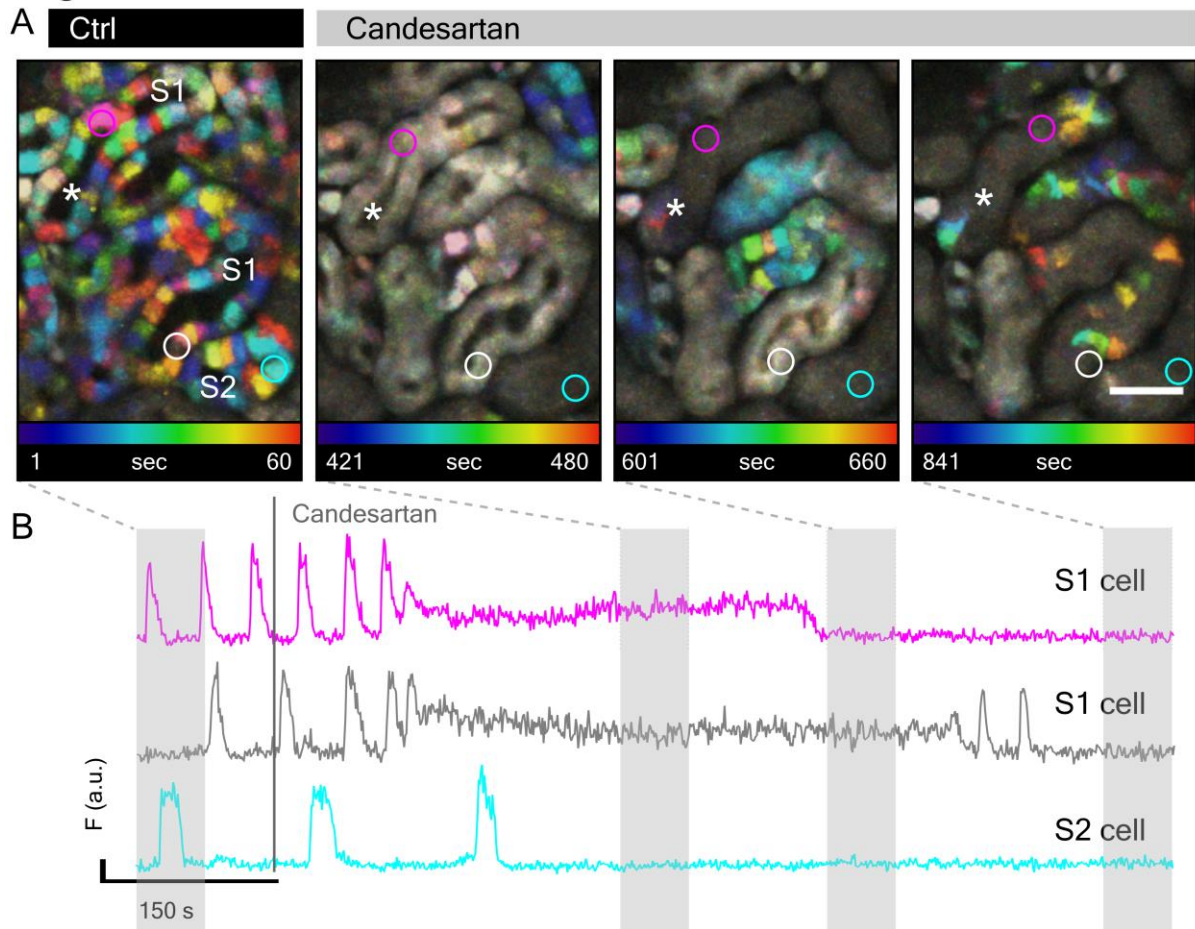


Fig. S6. Effect of candesartan on calcium transients in the proximal tubule. (A) Temporal color coded projections of GCaMP6s signal in the kidney, showing baseline Ca^{2+} transients in S1 and S2 proximal tubule (PT) cells within 60 sec. Upon intravenous injection of candesartan (60 $\mu\text{g}/\text{kg}$ body weight) PT lumens (*) collapse and transients are no longer detected. Representative of 4 independent experiments. Scale bars, 50 μm .

Movie S1. Co-imaging of calcium signaling and mitochondrial function in kidney proximal tubule cells. GCaMP6 signal (green) and the mitochondrial membrane potential dependent dye TMRM (grayscale), showing that spontaneous Ca^{2+} transients *in vivo* are not associated with changes in mitochondrial energization. Images were acquired at the rate of 1 frame per 5.41 sec. Scale bar, 50 μm .

Movie S2. Calcium transients originate apically and propagate towards the basolateral side of proximal tubule cells. GCaMP6s in grayscale (panel 1) and pseudocolor Spectrum (panel 2). GCaMP6s signal overlay with the mitochondrial membrane potential dependent dye TMRM (Mitoch, red) and SiRActin (Actin, cyan, panel 3), showing that Ca^{2+} transients *in vivo* originate beneath the apical brush border and propagate towards the basolateral side (cell indicated by arrow). Images were acquired at the rate of 1 frame per 0.68 sec. Scale bar, 20 μm .

Movie S3. Calcium transients in proximal tubules display a cyclical pattern in activation probability. Individual cells were grouped and mean activation probability within tubular segments calculated. Movie represents the moving average of 10 sec during a total recording period of 5 min. Tubular segments outlined in yellow correspond to S1 proximal tubular segments. Segments with activity but no outline are S2. Segments in white (S2 or distal tubule) displayed no transients during the recording period. Scale bar, 50 μm .

Movie S4. Proximal tubular cells show altered calcium signaling in cisplatin induced AKI. Detailed view of the GCaMP6s signal (orange hot) and the mitochondrial membrane potential dependent dye TMRM (grayscale) in proximal tubules from a 48h cisplatin treated

animal. Cells with high baseline Ca^{2+} and no transients can be observed bulging into the lumen (arrows, left panel). In another area a cell with high baseline Ca^{2+} sheds material into the lumen (right panel). Sequences were acquired at 1 frame per 5.41 sec (left panel) and 1 sec (right panel). Scale bars, 50 μm .

Movie S5. Cellular material is shed into tubular lumens in cisplatin induced AKI.

Detailed view of the GCaMP6s signal in a proximal tubule from a 72h cisplatin treated animal where cellular material with high Ca^{2+} can be observed moving in the lumen (*).

Sequence was acquired at 1 frame per 2 sec. Scale bars, 50 μm .

Supplementary Material and Methods

Immunofluorescence staining

Kidneys sections from 3 % Paraformaldehyde in 0.1 % Phosphate Buffer (0.2M NaH₂PO₄, 0.2M Na₂H PO₄, 0.1M CaCl₂) perfused animals were paraffin embedded and cut into 5 μm thick sections. Sections were deparaffinised and subjected to an antigen retrieval step using a citrate buffer. For confocal analysis and colocalization with NCC, frozen kidney sections from 3 % Paraformaldehyde in 0.1 % Phosphate Buffer (0.2M NaH₂PO₄, 0.2M Na₂H PO₄, 0.1M CaCl₂) perfused animals were cut at the cryostat into 5 μm thick sections.

After permeabilization with 0.1 % TritonX-100 (Surfact-Amps detergent solution; Thermo Fisher Scientific) for 2 min, tissue sections were blocked with 1% BSA and 10% donkey serum before incubation with primary antibodies (1:400 GFP, chicken polyclonal, Aves Labs and 1:10 000 NCC, rabbit polyclonal, kind gift from J Loffing lab (1)) overnight at 4°C. The secondary antibodies (1:300 Cy3 AffiniPure donkey anti chicken IgY (IgG), Jackson Immuno Research, USA, 1: 500 Alexa Fluor 647-conjugated AffiniPure Fab Fragment, donkey anti rabbit, Jackson Immuno Research, USA) were incubated for 2 h at RT. Tissue was subsequently washed with PBS, and cellular DNA was stained with 5 μg/ml Hoechst 33342 (Molecular Probes, Eugene, Oregon, USA, H1399) for 10 minutes at RT. Slices were mounted with Dako mounting medium (Agilent, Santa Clara, California, USA) and imaged.

Widefield imaging was done at a Axio Scan.Z1 Slide scanner (Zeiss), with a Plan Aplanachromat 20x/0.8 dry objective. Excitation was performed using a 550/25 bandpass filter, while emission was filtered with a 605/70 filter. Confocal imaging was performed at a IXplore SpinSR10a spinning disc (Olympus, Tokyo, Japan), with a UPlanSApo 40x/0.95 dry objective (Olympus, Tokyo, Japan) and spinning disk with 50 μm pinhole (Yokogawa, Japan). Excitation was performed sequentially using 405 nm, 561 nm and 640 nm lasers, while emission was filtered through the following bandpass filters: 447/60, 617/73 and 685/40. Images were processed using FIJI image analysis software and its plugins (2).

Cellular signal propagation

To evaluate the directionality of the intra cellular Ca²⁺ propagation, time series data was loaded in FIJI and line ROIs spanning the cell from the apical (AP) to the basolateral (BA) side were manually drawn. The temporal intensity profile data was exported using a custom FIJI macro. Further data analysis was performed in Wolfram Mathematica. First the abscissa of the line

profiles was rescaled from 0 to 1, corresponding to the normalized distance from AP to the BA side of the cell. Next, each intensity profile and time point was automatically assigned to one out of four possible states depending on the distribution of the cellular Ca^{2+} signal: Baseline, Apical High, Basolateral High, Overall High. To that end, an individual automated intensity threshold was calculated for each time series based on the signal intensity distribution together with a global scaling factor. Then the mean of the first 30% (AP) and last 30% (BA) of the intensity profile was calculated at each time point and compared to the threshold for assignment of the correspondent state. We then aggregated the states so that we could infer only the inter-state transitions and calculate the respective probabilities. The robustness of this approach has been validated by running the analysis using different scaling factors.

References

1. Loffing, J., Vallon, V., Loffing-Cueni, D., Aregger, F., Richter, K., Pietri, L., Bloch-Faure, M., Hoenderop, J. G., Shull, G. E., Meneton, P. *et al.* (2004) *J. Am. Soc. Nephrol.* **15**, 2276-2288.
2. Schindelin, J., Arganda-Carreras, I., Frise, E., Kaynig, V., Longair, M., Pietzsch, T., Preibisch, S., Rueden, C., Saalfeld, S., Schmid, B. *et al.* (2012) *Nat. Methods* **9**, 676-682.